Elsevier Editorial System(tm) for Journal of Catalysis
Manuscript Draft

Manuscript Number:

Title: Mechanism of CuCl2/γ-Al2O3 Ethylene Catalytic Oxidative Chlorination Into 1,2-Dichlorethane

Article Type: Research Article

Keywords: Structure, catalyst, oxidative chlorination, infrared spectroscopy, differential thermal analysis, mass spectroscopy, X-ray diffraction analysis, deactivation, compounds, iron

Corresponding Author: Professor Alex Volinsky, Ph.D.

Corresponding Author's Institution: University of South Florida

First Author: Sergey A Kurta, Ph.D.

Order of Authors: Sergey A Kurta, Ph.D.; Alex Volinsky, Ph.D.; Mykola S Kurta

***Covering Letter**

Dear Editor,

Please consider our original paper titled "Mechanism of $CuCl_2/\gamma$-Al_2O_3 Ethylene Catalytic Oxidative Chlorination Into 1,2-Dichlorethane" for publication in Journal of Catalysis.
The paper explains the mechanism of ethylene oxidative chlorination into 1,2-dichlorethane. This is original work not being considered for publication elsewhere.

Yours truly,
Alex Volinsky

***Referee Suggestions**

Fabrizio Cavani, Dipartimento di Chimica Industriale e dei Materiali, ALMA MATER STUDIORUM, Università di Bologna, Viale Risorgimento 4, 40136 Bologna, Italy

Ruud W. van den Brink, Center for Chemistry and the Environment, Leiden Institute of Chemistry, Gorlaeus Laboratories, Leiden University, P.O. Box 9502 2300 RA Leiden The Netherlands

J.-M. Giraudon, Unité de Catalyse et de Chimie du Solide, UMR CNRS 8181, USTL, Bâtiment C3, 59655 Villeneuve d'Ascq, France, Tel.: +33 3 20 43 68 56; fax: +33 3 20 43 65 61.

***Graphical Abstract**

Catalysis mechanism of ethylene $CuCl_2/\gamma\text{-}Al_2O_3$ oxidative chlorination into 1,2-dichlorethane

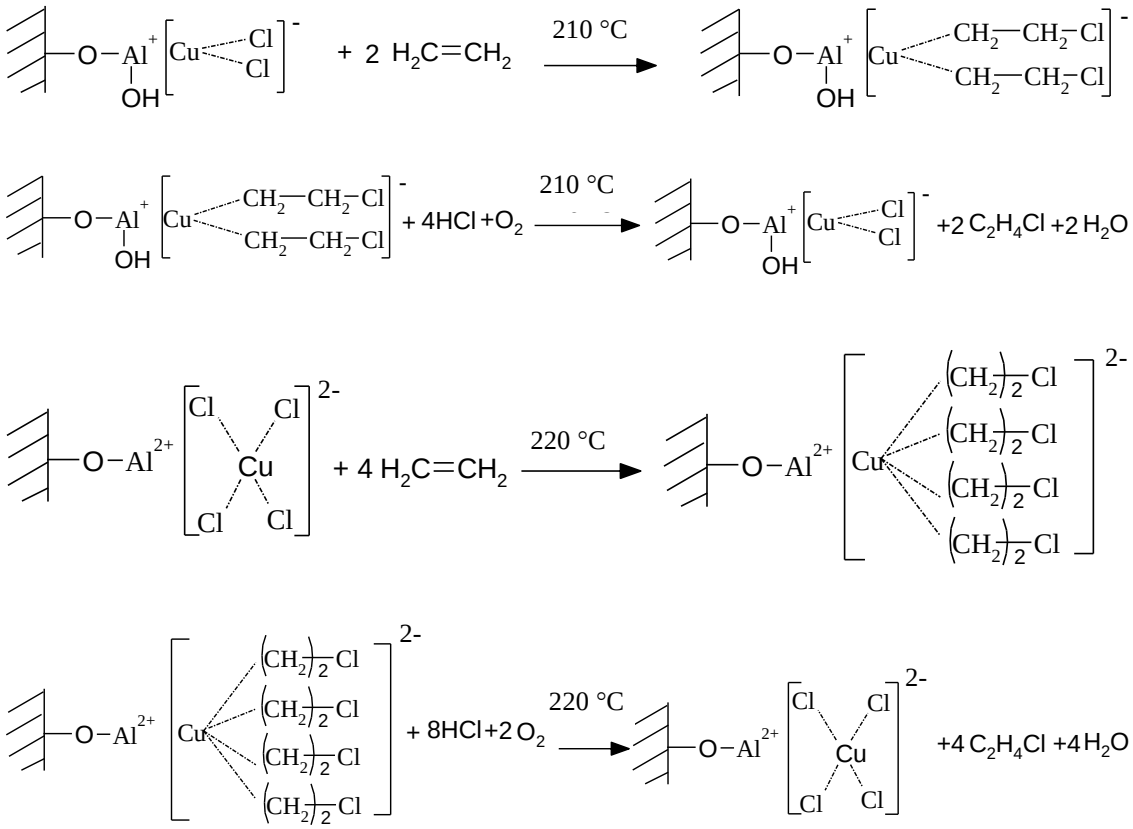

***Research Highlights**

Mechanisms of ethylene $CuCl_2/\gamma\text{-}Al_2O_3$ oxidative chlorination into 1,2-dichlorethane have been presented.

Mechanism of $CuCl_2/\gamma$-Al_2O_3 Ethylene Catalytic Oxidative Chlorination Into 1,2-Dichlorethane

S.A. Kurta[1], A.A. Volinsky[2], M.S. Kurta[2]
[1]Vasyl Stefanyk Precarpathian National University, Institute of Natural Science,
Department of Organic and Analytical Chemistry, 201 Galyska Str., Ivano-Frankivsk 76025, Ukraine
Phone: +38 0347252839, +38 0342723830, E-mail: kca2007@mail.ru
[2]Department of Mechanical Engineering, University of South Florida, Tampa FL 33620 USA

Abstract

Infrared spectroscopy and X-ray diffraction analysis were utilized to investigate the structure of the γ-Al_2O_3 carrier with $CuCl_2$ catalyst on its surface. Catalyst structure effects on the mechanism of ethylene oxidative chlorination reaction into 1,2-dichlorethane were studied. $CuCl_2$ catalyst interactions with γ-Al_2O_3 surface groups leads to $[CuCl_4]^{2-}$ and $[CuCl_2]^-$ complex compounds formation. Differential thermal analysis and mass spectroscopy were utilized to study the structure and the mechanism differences between the deposited and permeated $CuCl_2$ catalysts. Permeated catalyst exhibits better performance and selectivity than the deposited catalyst.

Keywords: structure, catalyst, oxidative chlorination, infrared spectroscopy, differential thermal analysis, mass spectroscopy, X-ray diffraction analysis, deactivation, compounds, iron.

1. Introduction

1,2-dichlorethane (1,2-DCE) forms as a result of ethylene oxidative chlorination (EOC) on the γ-Al_2O_3 surface with copper chloride catalyst. EOC reaction mechanism, qualitative and quantitative composition of reaction products can change depending on the catalyst. Ethylene oxidative chlorination into 1,2-DCE is conducted in the boiling layer of catalyst at 205-232 °C and 0.25-0.4 MPa pressure [1]:

$$C_2H_4 + 2HCl + 0.5O_2 \rightarrow C_2H_4Cl_2 + H_2O + Q \quad (1)$$

Secondary ethylene burning reactions also happen along with the main reaction:

$$C_2H_4 + 3O_2 \rightarrow 2CO_2 + 2H_2O \quad (2)$$
$$C_2H_4 + 2O_2 \rightarrow 2CO + 2H_2O \quad (2a)$$

According to references [2] the following reactions involving copper chlorides can occur:

$$2CuCl_2 + C_2H_4 \rightarrow C_2H_4Cl_2 + 2CuCl \quad (3)$$

$$2CuCl + O_2 \rightarrow Cu_2OCl_2 \quad (4)$$

$$Cu_2OCl_2 + 2HCl \rightarrow 2CuCl_2 + H_2O \quad (5)$$

Yet no report describes how copper chloride is bound to the γ-Al_2O_3 carrier surface [3], for it is well known that copper chloride by itself, without a carrier, does not catalyze ethylene oxidative chlorination reaction [4]. Therefore, without γ-Al_2O_3 surface groups involvement, reactions (3-5) proposed in reference [5] are not exact [6]. At the same time satellite reactions can occur, resulting in tetrachlorcarbon, chloral, chloroform, trichlorethane and other by-products that account for 1-2 wt.% of the produced 1,2-DCE:

$$C_2H_4 + 8HCl + 3O_2 \rightarrow 2CCl_4 + 6H_2O \quad (6)$$

$$C_2H_4 + 3HCl + 2O_2 \rightarrow C_2HCl_3O + 3H_2O \quad (7)$$

$$C_2H_4 + 6HCl + 2O_2 \rightarrow 2CHCl_3 + 4H_2O \quad (8)$$

$$C_2H_4 + 3HCl + O_2 \rightarrow C_2H_3Cl_3 + 2H_2O \quad (9)$$

2. Experiments

2.1 Materials

In order to study copper chloride effects on ethylene oxidative chlorination five samples were compared:

1) Pure γ-Al_2O_3 as a catalyst carrier;

2) Industrial X1 $CuCl_2$ catalyst (5 wt.% $Cu^{2+,1+}$, produced by Harshow Chemical Co, USA) applied from muriatic water solution on the γ-Al_2O_3 surface;

3) Industrial MEDC-B (OXYMAX-B) catalyst (5 wt.% $Cu^{2+,1+}$, produced by Montecatini Co, Italy or Sud-Chemie Catalysts) based on γ-Al_2O_3 permeated with $CuCl_2$;

4) $CuCl_2 \cdot 2H_2O$ – crystalline hydrate of the main catalyst component;

5) $CuCl_2 \cdot 2HCl$ – hydrochloride of the main catalyst component.

2.2 Methods

Obtained surface compounds were identified by means of Fourier transform infrared spectroscopy (FTIR, Thermo Nicolet Nexus 470, Thermo Electron Co, USA) in the 4000-400 cm^{-1} frequency range using diffuse reflectance attachment with 4 cm^{-1} resolution and 50 scans. KBr pellets were made with powder samples for analysis. Compounds thermal stability was studied using Paulic-Erday thermogravimetric system in the 25–1000 °C temperature range in air. X-ray diffraction patterns were obtained with a diffractometer using Cu-Kα radiation (λ= 1.54178 Å) with Bragg-Brentano focusing and Ni foil filter. Goniometer scan rate was 1 degree per minute. Samples were prepared by applying powders to a petroleum jelly amorphous layer on quartz substrates.

Mass spectrometry was carried out using monopole mass spectrometer (MX-7304A, Ukraine,1-210 mass range) with electron impact ionization, converted for thermal desorption measurements. Sample (0.1-20 mg) was placed at the bottom of a quartz-molybdenum vessel and pressure was reduced to $5 \cdot 10^{-5}$ Pa. Samples were heated to 750 ºC at 0.15 ºC per second. Volatile products entered the mass spectrometer ionization chamber where they were ionized and fragmented by electron beam. Desorption rate temperature dependence helps identifying thermal transformation products and provides interaction energy between the copper chloride active phase and γ-Al_2O_3 carrier [7].

3. Results and Discussion

3.1. Infrared spectra of the carrier, catalyst and copper chloride

Infrared spectra from γ-Al_2O_3 carrier, $CuCl_2 \cdot 2H_2O$ and $CuCl_2 \cdot 2HCl$ main catalyst components, industrial MEDC-B and X1 catalysts are shown in Fig. 1. Most interesting characteristics of the catalyst surface groups on γ-Al_2O_3 are in the 1640-1377 cm^{-1} range. In this range triplet absorption bands are attributed to (-OH) groups vibrations of structured water in $Al_2O_3 \cdot nH_2O$ or $Al(OH)_3$ [8], and water in $CuCl_2 \cdot 2H_2O$. There are also (-OH) groups deformation vibrations of $Al^{+2}OH$ on the γ-Al_2O_3 surface at 1518 cm^{-1} and $Al^{+}(OH)_2$ at 1377 cm^{-1}, which coincide in intensity. At the same time there are hardly any (-OH) groups vibrations of $Al^{2+}OH$ and $Al^{+}(OH)_2$ on the γ-Al_2O_3 surface at 1518 cm^{-1} and 1377 cm^{-1} for MEDC-B and X1 commercial catalysts. This confirms the existence of interactions between $Al^{2+}OH$ and $Al^{+}(OH)_2$ surface groups and copper chloride or complex copper compounds $[CuCl_4]^{2-,1-}$. Moreover, X1 catalyst shows residual absorption intensity due to $Al^{+1}(OH)_2$ type (-OH) group vibrations at 1377 cm^{-1}. This may indicate that when $CuCl_2$ is deposited on the γ-Al_2O_3 surface, it leads to two types of complex compounds formation between $Al^{+2}OH$ and $[CuCl_4]^{2-,1-}$, and partially with $Al^{+}(OH)_2$.

For the MEDC-B catalyst there are absorptions at 1518 cm^{-1} and 1377 cm^{-1}, which indicate that all $Al^{+2}OH$ and $Al^{+1}(OH)_2$ groups interact with $[CuCl_4]^{2-,1-}$ catalyst. However, MEDC-B and X1 catalysts exhibit another absorption band at 1277 cm^{-1}, which is not found on the γ-Al_2O_3 carrier surface. This indicates restructuring in the catalyst surface layer due to the formation of new copper chloride complex compounds $[CuCl_4]^{2-,1-}$ with γ-Al_2O_3 surface groups.

$CuCl_2 \cdot 2H_2O$ and $CuCl_2 \cdot 2HCl$ spectra in Fig. 1 suggest the following. $CuCl_2 \cdot 2HCl$ is characterized by dual absorption bands related to valence vibrations of the H···Cl hydrogen bonds at 3230 cm^{-1} and 3196 cm^{-1}, which are hardly found in the $CuCl_2 \cdot 2H_2O$ compound spectrum, where hydrogen bonds clearly manifest themselves at 3680 cm^{-1}.

At the same time $CuCl_2 \cdot 2HCl$ infrared spectrum clearly shows deformation vibrations frequency of the H···Cl hydrogen bonds at 1595 cm^{-1}, whereas $CuCl_2 \cdot 2H_2O$ spectrum reveals deformation vibrations of the O···H bonds absorption frequency at 1620 cm^{-1}. Besides, these two compounds are characterized by a distinctive vibration frequency in the 1320-1277 cm^{-1} range, which can be ascribed to deformation vibrations of H···Cl in H_2CuCl_4 or $HCuCl_2$ complex metal compounds. Interestingly, these compounds are also identified in the same 1277-1250 cm^{-1} range for MEDC-B and X1 catalysts, which prove the existence of complex metal compounds on the catalyst surface. However, due to their interactions with the carrier surface, vibration frequencies are shifted into a lower 1277-1250 cm^{-1} range of the infrared spectrum. This leads to an assumption that there are complex metal compounds with copper of the $[CuCl_4]^{2-}$ and $[CuCl_2]^{-}$ type on the MEDC-B and X1 catalysts surfaces, confirmed by the data from other sources [9]. Such complexes can form according to the following mechanism. It is known that copper chloride in hydrochloric acid solution forms complex di- and tetra- copper chlorides [10]:

$$CuCl_2 + 2HCl \rightarrow H_2[CuCI_4] \quad (10)$$

$$Cu_2Cl_2 + 2HCl \rightarrow 2H[CuCI_2] \quad (11)$$

It is also known from literature sources that copper chloride deposition on γ-Al_2O_3 surface is conducted from $CuCl_2$ solutions in hydrochloric acid [11]. Thus it is complex copper tetrachloride that is deposited on the γ-Al_2O_3 surface following reactions 10 and 11 [12], rather than $CuCl_2$. Taking into account results

from reference [10], copper tetrachloride has a flat square structure and can easily fit between Al_2O_3 layers in pores and on surfaces of γ-Al_2O_3 (Figure 2).

While $[CuCl_4]^-$ has a flat plane structure, $CuCl_2$ is linear, which is why it easily coordinates with the γ-Al_2O_3 surface (Figure 2b). Also complex copper tetrachloride and dichloride can have three hybridization types. In the ground state Cu atom has the following electron configuration:

Cu° $1s^2 2s^2 2p^6 3s^2 3p^6 3d^{10} 4s^1 \rightarrow 3d^{10}$ ↑↓ ↑ ↑ ↑ ↑ ↑ $4s^1$ ↑ $4p^0$ □ □ □

The three Cu hybridizations are:

1) sp: $Cu^\circ - 1\bar{e} \rightarrow Cu^{+1}$ ... $3d^{10}4s^0 \rightarrow 3d^{10}$ ↑↓ ↑↓ ↑↓ ↑↓ ↑↓ $4s^0$ □ $4p^0$ □ □ □ $+ 2Cl^- \rightarrow$

$\rightarrow [CuCl_2]^-$ $3d^{10}$ ↑↓ ↑↓ ↑↓ ↑↓ ↑↓ $4s^2$ ↑↓ $4p^2$ ↑↓ □ □

2) sp^3: $Cu^\circ - 2\bar{e} \rightarrow Cu^{2+}$ ... $3d^9 4s^0 \rightarrow 3d^9$ ↑↓ ↑↓ ↑↓ ↑↓ ↑ $4s^0$ □ $4p^0$ □ □ □ $+ 4Cl^- \rightarrow$

$\rightarrow [CuCl_4]^{2-}$ $3d^9$ ↑↓ ↑↓ ↑↓ ↑↓ ↑ $4s^2$ ↑↓ $4p^6$ ↑↓ ↑↓ ↑↓

3) sp^2d: $Cu^\circ - 2\bar{e} \rightarrow Cu^{2+}$ ... $3d^9 4s^0 \rightarrow 3d^9$ ↑↓ ↑↓ ↑↓ ↑↓ ↑ $4s^0$ □ $4p^0$ □ □ □ $+ 4Cl^- \rightarrow$

$\rightarrow [CuCl_4]^{-1}$ $3d^{10}$ ↑↓ ↑↓ ↑↓ ↑↓ ↑↓ $4s^2$ ↑↓ $4p^4$ ↑↓ ↑↓ □

Moreover, sp and sp^3 complexes have external hybridization and thus are paramagnetic, while sp^2d complexes are diamagnetic. Sp and sp^2d complexes are linear, while sp^3 complex has tetrahedral configuration. Sp and sp^3 complexes with external hybridization are more reactive than sp^2d complex with internal hybridization, which reacts at higher temperatures [10].

Infrared spectroscopy results showed that Al_2O_3 surface is partly hydrated with aluminium hydroxyl groups formation. That is why it is assumed that the followings reactions between $Al^{2+}OH$ and $Al^+(OH)_2$ carrier surface groups, and $H_2[CuCl_4]$ and $H[CuCl_2]$ catalyst compounds are possible:

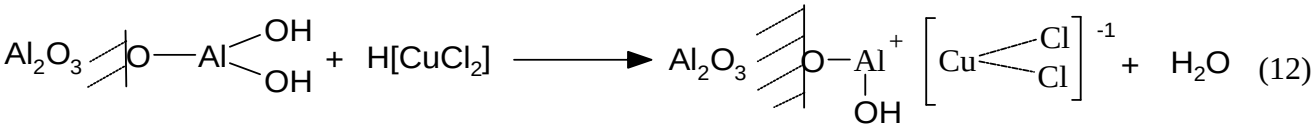

(12)

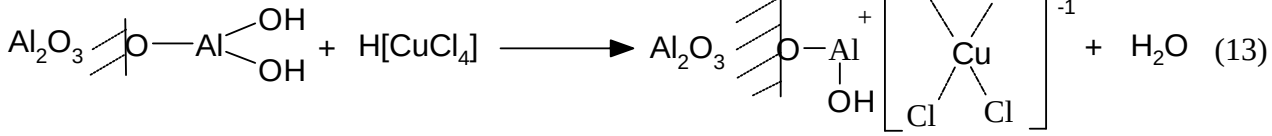

(13)

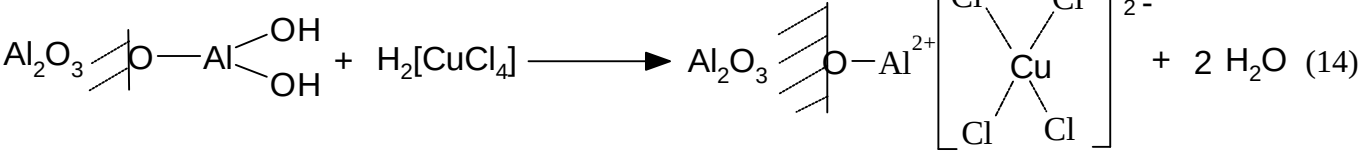

(14)

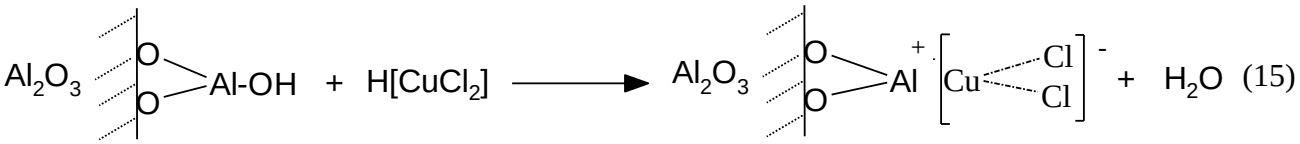

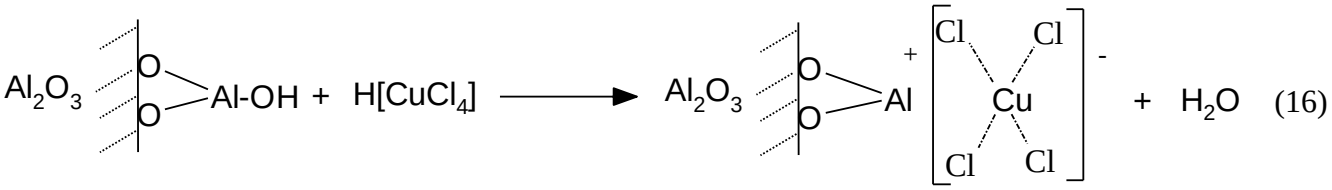

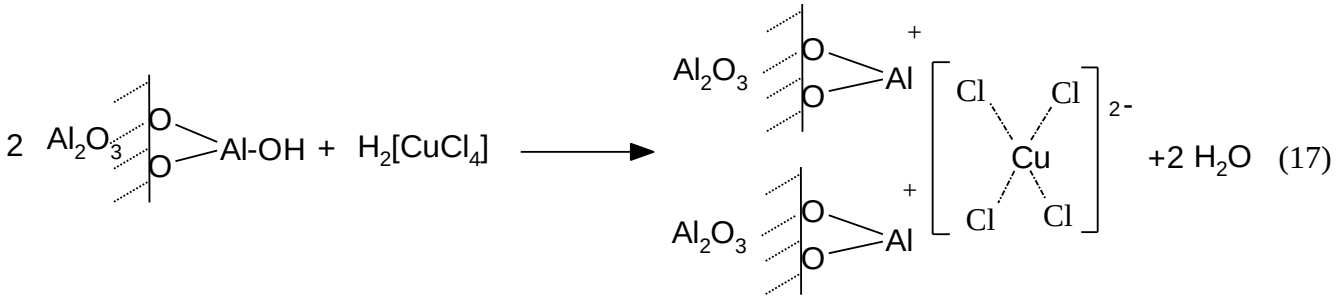

Three types of compounds are formed during ethylene oxidative chlorination catalyst surface reactions 12-17 between hydrated Al_2O_3 and copper complexes $[CuCl_4]^{2-}$, $[CuCl_2]^{-}$ and $[CuCl_4]^{-}$, identified by wide absorption bands in the 1277-1250 cm^{-1} range. Absorption frequencies in the catalyst infrared spectra disappear for $Al^{+}(OH)_2$ surface groups at 1377 cm^{-1} and for $Al^{2+}OH$ at 1578 cm^{-1}.

Based on the spectral analysis it is possible to say that the intensity of interactions between $CuCl_2$ and γ-Al_2O_3 is higher for catalyst MEDC-B than for catalyst X1. This difference is presumably caused by their preparation methodology. MEDC-B preparation technology by mechanical chemical activation of amorphous γ-Al_2O_3 and crystalline $CuCl_2$ from muriatic solutions forming 20-120 μm diameter catalyst micro-particles results in more intense interactions and in complex compounds formation on surfaces, in pores and catalyst microstructure (reactions 14, 16 and 17). At the same time during $CuCl_2$ deposition from muriatic solution on the hard γ-Al_2O_3 particles surface (X1 catalyst) ordinary $[CuCl_4]^{2-,1-}$ adsorption happens. As a result of this interaction only partially coordinated bonds are formed between γ-Al_2O_3 carrier (X1) and deposited catalyst (reactions 12, 13,15 and 16), while copper appears in the form of individual copper chloride compounds (reactions 10 and 11). That is why in 1-2 years of X1 service most of the $[CuCl_4]^{2-,1-}$ catalyst is gone from the γ-Al_2O_3 surface resulting in the catalyst efficiency loss for ethylene oxidative chlorination into 1,2-dichlorethane [6].

Oppositely, wear resistant hard surfaces of the MEDC-B catalyst cause wear of metal walls in industrial reactors, worm pipes and cyclones. As a result many plants producing 1,2-dichlorethane have to increase the thickness and durability of metal walls in reactors and other processing apparatus [13]. At the same time it is known that reactor walls and surfaces of cooling and heating worm pipes are covered with a thick layer of metallic copper [14], which is reduced from $[CuCl_4]^{2-,1-}$:

$$Fe + H_2[CuCl_4] \rightarrow FeCl_2 + Cu + 2HCl \quad (18)$$

$$Fe + CuCl_2 \rightarrow FeCl_2 + Cu \quad (19)$$

This results in quite severe MEDC-B catalyst contamination by iron chlorides and oxides which are hard to remove from the catalyst surface [15]:

$$FeCl_2 + H_2[CuCl_4] \rightarrow FeCl_3 + H[CuCl_2] + HCl \quad (20)$$

$$FeCl_2 + H[CuCl_2] \rightarrow FeCl_3 + Cu + HCl \quad (21)$$

$$2FeCl_2 + 2HCl + 1/2O_2 \rightarrow 2FeCl_3 + H_2O \quad (22)$$

$$FeCl_2 + CuCl_2 \rightarrow FeCl_3 + CuCl \quad (23)$$

$$2FeCl_3 + 3H_2O \leftrightarrow Fe_2O_3 + 6HCl \quad (24)$$

3.2. Differential thermal analysis of the carrier, catalyst and copper chloride

For a detailed identification of the active centres, differential thermal analysis results of the γ-Al_2O_3 carrier samples with X1 and MEDC-B catalysts were interpreted [16]. These results are summarized in Table 1.

Differential thermal analysis curves of the γ-Al_2O_3 carrier have three distinct regions upon heating. The first region is γ-Al_2O_3 drying, which begins at 25-50 °C and completes at about 120 °C. The highest drying rate is at 120 °C, which is characteristic of removing adsorbed water from the powder carrier surface at normal pressure, a highly endothermic process. Physically adsorbed water losses on the γ-Al_2O_3 surface are about 4 wt.% with 2.34 mg/min drying rate. Past 120 °C dehydration processes begin with γ-Al_2O_3 catalyst surface structure and composition change, signified by the exothermic curve in the 120-250 °C temperatures range. Obviously at these temperatures γ-Al_2O_3 dehydration with partial loss of water and hydroxyl groups (-Al-$(OH)_{n=1,2}$) from the bulk begins. Further heating above 250 °C leads to γ-Al_2O_3 structural transformations, sintering and sample destruction. The total weight loss of γ-Al_2O_3 at 950 °C is 12 wt.%.

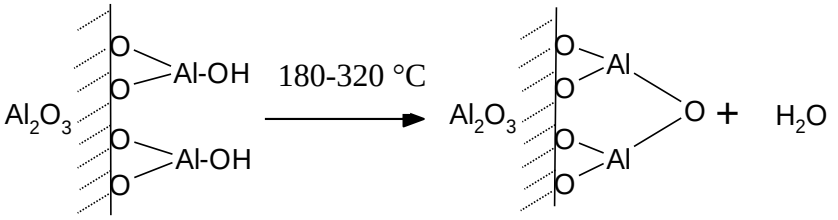

dehydration (25)

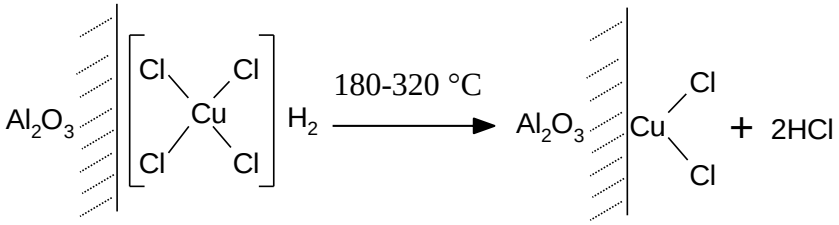

dehydrochlorination (26)

X1 catalyst consists of γ-Al_2O_3 surface with deposited $[CuCl_4]^{-1,-2}$ active phase, and its transformation temperature ranges are different (Table 1). Drying and dehydration happen between 20 °C and 180 °C. X1 dehydration and dehydrochlorination (reactions 25 and 26) start at 180 °C and end at 250

°C, higher than γ-Al_2O_3 high rate dehydration temperature. At the same time desorption rate of 2.23 mg/min is lower, and total dehydratation and dehydrochlorination rate grows to 2.31 mg/min in the 180-250 °C range. Reactions 25 and 26 result in γ-Al_2O_3·$[CuCl_4]^{2+,1+}$ surface layer modifications with 5.72 wt.% loss during desorption and 2.6 wt.% loss during dehydratation and dehydrochlorination. Further X1 heating from 250 to 550 °C results in more weight loss, up to 9.49 wt.%. The total weight losses at 900 °C are about 20 wt.% with 1.97 mg/min weight loss rate above 550 °C.

The difference between X1 total 20.55 wt.% weight loss and 8.32 wt.% desorption, dehydratation and dehydrochlorination combined losses up to 350 °C is about 12 wt.%, which accounts for the most $[CuCl_4]^{2-,1-}$ active phase loses. Above 500 °C copper chlorides decompose following reactions 18, 19 and 21 causing weight loss in the 500-600 °C range. To summarize, copper chlorides active phase is stable on the X1 catalyst surface in the 180-250 °C range. Above 180-250 °C $[CuCl_4]^{2-,1-}$ active phase is destroyed, and above 320 °C there is $CuCl_2$ and CuCl destruction resulting in $Cu_2(O)Cl_2$ (reaction 4), and CuO formation [5].

For the MEDC-B catalyst dehydration, dehydration and dehydrochlorination processes happen at higher temperatures compared with X1. The maximum dehydration rate is in the 21-200 °C range is 20 °C higher than for the X1 catalyst. The same can be said about dehydration and dehydrochlorination processes in the 200-250 °C range. At the same time dehydration rate reduces by a factor of two to 1.33 mg/min, while dehydration and dehydrochlorination rate exceeds 3 mg/min. Dehydration weight losses are reduced to 3.93 wt.%, while dehydration and dehydrochlorination weight losses of 2.54 wt.% are comparable with X1 catalyst.

The main conclusion comparing DTA results for X1 and MEDC-B catalysts is that dehydration and dehydrochlorination ranges are different. For X1 the range is 180-250 °C (ΔT=70 °C), and for MEDC-B catalyst it is 200-250 °C (ΔT=50 °C). Working temperature range of 215-220 °C is narrower for MEDC-B catalyst compared with X1 catalyst, which is advantageous for ethylene oxidative chlorination into 1,2-dichlorethane, thus $CuCl_2$ permeated MEDC-B catalyst has better selectivity.

$CuCl_2$ deposited X1 catalyst has a wide 190-210 °C reaction temperature range, which in large scale production causes ethylene oxidative chlorination side reactions into trichlorethane, tetrachlorethane and perchlorethylene, as well as ethylene combustion. This is proven by the fact that X1 $CuCl_2$ deposited catalyst selectivity does not exceed 95-97%, while with MEDC-B permeated $CuCl_2$ catalyst it increases to 97-99%. Industrial practice shows that ethylene combustion into CO and CO_2 with MEDC-B permeated catalyst is reduced to 1.5-2%, compared to X1 deposited catalyst, where ethylene combustion reaches up to 3-5% [17].

Comparing catalyst selectivity of ethylene oxidative chlorination into 1,2-DCE and ethylene combustion, the amount of impurities (trichlorethane, trichloroethylene, etc. side products) is 1-1.5% for MEDC-B and 1.5-2.5% for X1 catalyst, which confirms DTA analysis conclusions. X1 deposited catalyst significantly catalyses the process of ethylene combustion due to the influence of the γ-Al_2O_3 surface deprived of the active $[CuCl_4]^{2-,1-}$ phase [18]. In MEDC-B permeated catalyst the active phase is evenly distributed in the γ-Al_2O_3 structure and reduces the carrier's influence on the ethylene combustion reaction. These effects are observed in industrial processes of ethylene oxidative chlorination into 1,2-DCE [22].

3.3. X-ray phase analysis of the carrier, catalyst and copper chloride

X-ray phase analysis of the carrier and the catalyst was carried out (Fig. 3). It shows that air exposure of copper chloride causes oxychlorides formation following reaction 4, as predicted in reference [5]. X1 catalyst diffraction pattern differs from that of the initial γ-Al_2O_3 sample in Fig. 4 [17]. These differences consist of 25-27% decreased 36.65°, 45.9° and 66.9° reflection intensities. Decreased reflections intensities are due to the presence of other phases in the sample, namely $[CuCl_2]^-$, $[CuCl_4]^{2-}$, which interact with the γ-Al_2O_3 surface groups and decrease the intensity. Furthermore, X1 catalyst sample exhibits a new reflection around 28.55° (Fig. 4). This reflection corresponds to the new $CuCl_2$ phase [17], although diffraction angle positions do not coincide with the corresponding reflections of the pure $CuCl_2$ diffraction pattern. This suggests that copper chloride adsorption on the γ-Al_2O_3 surface interacts with alumina and 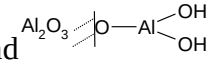 hydroxyl surface groups. Comparing diffraction patterns in Fig. 4, pure X1 catalyst does not contain copper hydroxychloride which corresponds to 32.4°, 36.65° and 39.25° 2θ reflections. After X1 catalyst air exposure its diffraction pattern shows an additional reflection at 16.1°, which is not found in the pure sample diffraction pattern, even after air exposure (Fig. 3). This can be explained by the formation of copper hydroxides and mixed hydroxychlorides Cu(OH)Cl or $Cu(OH)_2$ and $CuCl_2 \cdot 2H_2O$ due to water vapour in air [5].

MEDC-B catalyst diffraction pattern (Fig. 4) suggests that as with the X1 catalyst, copper chloride application onto the γ-Al_2O_3 surface also proportionally decreases 37.1°, 45.75° and 67° 2θ reflections intensity by 25%. Such intensity decrease indicates the presence of $[CuCl_2]^-$, $[CuCl_4]^{2-}$, and Cu(OH)Cl phases in the MEDC-B catalyst which interact with Al_2O_3 surface groups. In contrast to the X1 catalyst, there is no crystalline $CuCl_2$ reflection at 28.55° for the MEDC-B catalyst (Fig. 4). This leads to the conclusion that all active copper chloride is evenly distributed throughout all MEDC-B catalyst particles volume and bound to the Al_2O_3 surface.

From the diffraction data presented in Tables 2 and 3, it is clear that the structure of the $CuCl_2$ catalyst surface compounds on the γ-Al_2O_3 carrier is different for the X1 and MEDC-B catalysts. Based on the MEDC-B catalyst similar 32°, 37° and 39° reflections intensity one can speak of the same structure of the catalyst and the carrier surface compounds, for example, $[CuCl_2]Al(OH)_2$, $[CuCl_4]AlO$, $[CuCl_4]Al(OH)$ investigated earlier [6].

At the same time, X1 catalyst 32°, 37° and 39° intensities differ greatly (Table 2, Fig. 4). This indicates the presence of at least three, and possibly more different compounds between $CuCl_2$ and γ-Al_2O_3 on the X1 catalyst surface confirmed by the literature sources [19]. Data presented in Tables 2 and 3, which show the inter-planar spacing difference (Δd) for the catalyst carrier (d_{Al2O3}), X1 catalyst (d_{X1}, Table 2) and MEDC-B catalyst ($d_{MEDC\text{-}B}$, Table 3), suggest the following.

X1 catalyst, if compared to the γ-Al_2O_3 carrier, is characterized by the inter-planar spacing increase for the characteristic 28.55º, 36.55º, 39.25º, 45.9º and 79.7º diffraction lines, which is an indication of a wedging effect of the excess pure $CuCl_2$+CuCl crystal phase [3]. In contrast, MEDC-B catalyst, if compared to the γ-Al_2O_3 carrier, is characterized by the inter-planar spacing decrease for 20.55º; 32.6º; 39.45º and 68.0º diffraction lines, which is an indication of homogeneity of phases of the catalyst and the carrier, in which the catalyst is present both on the surface and in the structure without $CuCl_2$ crystal phase.

3.4. Mass spectrometry of the carrier, catalyst and copper chloride

X1 and the MEDC-B catalysts, the γ-Al_2O_3 carrier, active $CuCl_2 \cdot H_2O$ and $CuCl_2 \cdot 2HCl$ or $H_2[CuCl_4]$ phases were analyzed using temperature-programmed desorption mass spectrometry to identify individual thermal transformation products on the catalyst surface, the carrier and the copper chloride active phase. Mass spectrometry curves (Figs. 5-9) represent qualitative and quantitative compounds analyses desorbed from the sample surface.

As predicted by DTA and infrared spectroscopy, maximum desorption of the physically bound water from the carrier (Fig. 5) and the catalysts (Fig. 6, 7) surfaces starts at 100 °C, identified by the molecular weight of water H_2O (M_{H2O}=16-18). Besides, in the same curves one can identify small desorption peaks for carbon dioxide CO_2 (M_{CO2}=44), which are more characteristic of the carrier and less of the catalyst, with maximum desorption at about 80 ˚C. Products desorption from catalysts is much more complicated, however.

X1 catalyst exhibits ethylene desorption at 100-150˚C (M_{C2H4}=28), which is hardly found in the MEDC-B catalyst. Main transformations on the catalyst surface start above 150 °C. With the MEDC-B catalyst, the maximum HCl loss (M_{HCl}=35-38) is observed at 140 °C, where several desorption peaks belonging to HCl can be identified. The difference between them can be explained by different desorption rate of HCl of different origin from the catalyst surface, which can be the result of its release from different places on the catalyst surface and from its internal structure, or due to $CuCl_2 \cdot 2HCl$ or $H_2[CuCl_4]$ and $CuCl_2 \cdot H_2O$ decomposition.

At the same time, similar HCl desorption peaks for both catalysts are observed again at a higher temperature. For the X1 catalyst this area corresponds to the desorption temperature of 260 °C and for the MEDC-B catalyst the maximum is reached at 270 °C. Obviously, in this temperature range ethylene oxidative chlorination reaction occurs: 210-260 °C for X1 and 220-270 °C for MEDC-B catalysts. Besides, in this range water loss is also observed, produced as a result of $CuCl_2 \cdot H_2O$ dehydration reaction 25 [15].

It is considered that copper chlorides catalyst active phase dehydrochlorination occurs according to reaction 26. Since the peak intensity of HCl loss in the 220-270 °C range is almost twice higher with the MEDC-B catalyst (Fig. 6) than with the X1 catalyst (Fig. 7), one can assume a more intense ethylene oxidative chlorination reaction with the permeated MEDC-B catalyst.

Desorption curves analysis of the active $CuCl_2 \cdot H_2O$ phase (Fig. 8) and $CuCl_2 \cdot 2HCl$ or $H_2[CuCl_4]$ phases (Fig. 9) suggests the following. In the 100-200 °C temperature range partially hydrolyzed $CuCl_2 \cdot H_2O$ active phase looses large amounts of adsorbed and structured water. Internally crystallized water release starts at 170 °C, while adsorbed water release starts above 50 °C, which is not observed with a pure $CuCl_2 \cdot 2HCl$ or $H_2[CuCl_4]$ active phase. Intensive dehydrochlorination processes of the $CuCl_2 \cdot H_2O$ active phase occur in the 200-300°C range identified by maximum HCl desorption peaks at 260 °C for both types of active phases. However, with pure non-hydrolyzed $CuCl_2 \cdot 2HCl$ or $H_2[CuCl_4]$ phases dehydrochlorination processes intensity is higher and consists of 3 peaks, whereas with a partially hydrolyzed $CuCl_2 \cdot H_2O$, it consists of only 2 HCl desorption peaks (M_{HCl}=35-38). Still, the most interesting characteristic of the active phase decomposition products is the intense molecular chlorine Cl_2 desorption peak (M_{Cl2}=70), which is two times more intense with a pure active $H_2[CuCl_4]$ phase. This phenomenon has not been observed before with other analysis methods [5] and provides evidence of the active phase decomposition reaction with Cl_2 release (reactions 27 and 29), which may be involved in ethylene chlorination reactions 1-5 [17].

$$H_2[CuCl_4] \xrightarrow{220^{\circ}C} H_2[CuCl_2] + 1/2Cl_2 + HCl \quad (27)$$

$$H_2[CuCl_4] \xrightarrow{235\ ^{\circ}C} 2HCl + CuCl_2 \quad (28)$$

Literature sources describe similar phenomenon of chlorine release from the catalyst active phase when copper dichloride turns into copper monochloride [10]:

$$2CuCl_2 = 2CuCl + Cl_2 \quad (29)$$

All of the above confirms the structure of active centres on the X1 and MEDC-B catalysts surface presented by reactions 12-17. Besides, HCl and Cl_2 release according to reactions 27-29 in the processes of the active phase thermal destruction in the 210-235 °C working temperature range confirms the EOC reaction mechanism described in [16] and presented below.

3.5. Predicted EOC reaction mechanisms on the catalyst surface

Based on the X-ray phase analysis and earlier presented electron microscopy results [16], infrared spectroscopy and differential thermal analysis of the Al_2O_3 carrier samples with X1 and MEDC-B catalysts, the following catalysis mechanism of the surface EOC process is suggested:

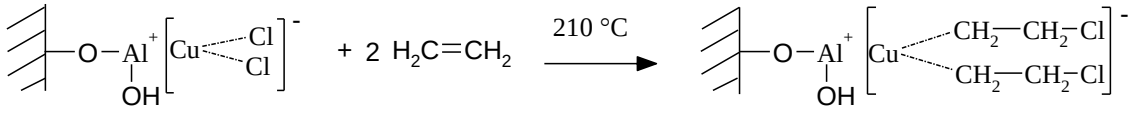

(30)

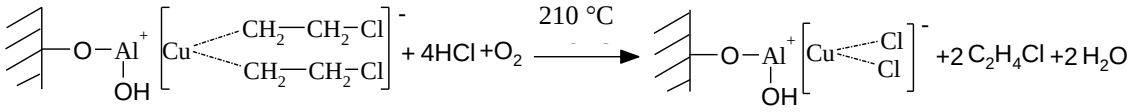

(31)

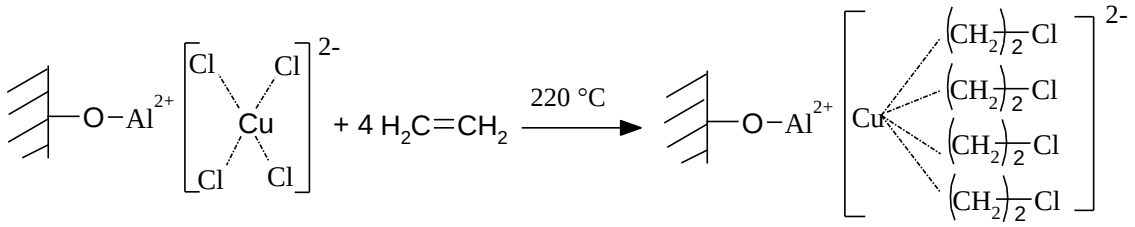

(32)

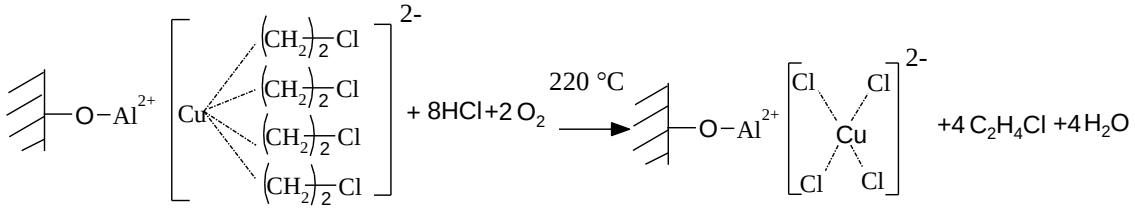

(33)

Based on the literature data indicating the existence of an independent $CuCl_2$ phase [20] and complex $[CuCl_2]^{2-,1-}$ compounds on the X1 OCE catalyst surface [21], one can predict X1 catalysis mechanism represented by reactions 30 and 31. Since all copper on permeated MEDC-B catalyst is in the form of complex $[CuCl_4]^{2-}$ compounds, which evenly interact with the carrier surface groups shown by reactions 14 and 17, one can predict that prevailing MEDC-B catalysis mechanism is represented by reactions 32 and 33.

These mechanisms are also confirmed by X1 and MEDC-B catalysts industrial use [6]. It is known that with the X1 deposited catalyst 1,2-DCE yield is 1.5-1.7 times smaller than with the permeated MEDC-B catalyst, evident from reactions 30-33. Besides, it also known from industrial practice that with the X1 deposited catalyst type the ratio of the main OCE reaction agents $HCl{:}C_2H_4{:}O_2$ is (1.9-2):(1):(0.7-0.8), whereas with the permeated MEDC-B atalyst this ratio increases for hydrogen chloride and ethylene and decreases for oxygen $HCl{:}C_2H_4{:}O_2$ = (2-2.2):(1-1.2):(0.5-0.6), which contributes to 1,2-DCE yield increase per unit of catalyst area. This is only possible if the catalyst has higher production capacity in terms of 1,2-DCE yield per 1 ton of catalyst, which increases by 1.5-2 with the MEDC-B catalyst use [17].

4. Conclusions

The following conclusions can be drawn.

1. Structure of $CuCl_2$ active catalyst centres used for ethylene oxidative chlorination on the γ-Al_2O_3 carrier was described, namely two types of catalysts were considered: deposited X1 catalyst and permeated MEDC-B catalyst. $CuCl_2$ interactions with γ-Al_2O_3 surface groups (≡Al-OH) lead to complex compounds formation with $[CuCl_4]^{2-}$ and $[CuCl_2]^{-}$.
2. A new mechanism of metal-complex catalysis of the ethylene oxidative chlorination reaction into 1,2-dichlorethane with $Al_2O_3[CuCl_4]^{2-}$ and $Al_2O_3[CuCl_2]^{-}$ surface metal complexes reacting with ethylene, hydrogen chloride and oxygen was proposed.
3. It was shown that contamination and deactivation of the EOC catalyst occurs due to the accumulation of iron compounds on the catalyst surface in the form of $Fe^{3+,2+}{\cdot}nH_2O$ (or ·nHCl), mainly caused by the reactor contamination in the course of chemical interaction of Cu(II), (I) with iron reactor walls.
4. Differential thermal analysis simulates catalysts' industrial tests. MEDC-B catalyst has higher dehydration and dehydrochlorination rate, and higher 210-220 °C EOC temperature range compared with X1 catalyst (200-210 °C). MEDC-B catalyst is more stable, but less active in the lower 190-210 °C EOC temperature range, thus its optimal EOC temperature range is 210-220 °C.
5. Lower total weight loss of 17% during MEDC-B catalyst heating compared with 20% for X1 is caused by the smaller amounts of the adsorbed and structured water, and by smaller dehydrochlorination losses.
6. MEDC-B catalyst dehydration rate increases as a result of $[CuCl_4]^{2-,1-}$ and Al_2O_3 interactions. Modified $[CuCl_4]^{2-,1-}$ catalyst acts as chlorine transmitter during its reduction and dehydrochlorination in the 200-250 °C range, which is within the 215-225 °C range of ethylene oxidative chlorination catalyst working temperature.
7. X1 catalyst dehydration and dehydrochlorination temperature range is 180-250 °C (ΔT=70 °C), while for MEDC-B it is 200-250 °C (ΔT=50 °C). Working temperature range reduction by 20 °C for MEDC-B compared with X1 catalyst is beneficial for ethylene oxidative chlorination reaction into 1,2-DCE and significantly increases process selectivity. Deposited X1 catalyst has a larger 190-210 °C working temperature range, which causes side reactions of ethylene combustion and oxidative chlorination into trichloroethylene. While X1 catalyst selectivity does not exceed 95-97%, MEDC-B

selectivity is 97-99%. Based on industrial tests ethylene combustion to CO and CO_2 diminishes to 1.5-2% for MEDC-B. For the permeated MEDC-B catalyst active phase is evenly distributed throughout γ-Al_2O_3 structure, which diminishes carrier influence on ethylene combustion observed in industrial EOC technological processes.

References

1. J.A. Allen., A.J. Clark, Rev. of Pure and Appl. Chem. 21 (1971) 145.
2. J.S. Naworski, E.S. Evil, (B.E. Leach, Ed.), Applied Industrial Catalysis Vol. 1, Accademic Press, New York, 1983, p. 239.
3. C. Lamberti, C. Prestipino, L. Capello, S. Bordiga, A. Zecchina, G. Spoto, S.D. Moreno, A. Marsella, B. Cremaschi, M. Garilli, S. Vidotto, G. Leofanti, Int. J. Mol. Sci. 2 (2001) 230-245.
4. S.A. Kurta, I.M. Mykytyn, N.V. Khaber, P.T. Skakun, Ukraine Patent 88262, Method of Obtaining Catalysts for Oxidative Chlorination of Ethylene into 1,2-Dichlorethane, 12.12.2007, declared on 25.06.2009, published Bulletin No. 9, 12.10.2009.
5. M.D. Flid, Yu.A. Treger, Vinyl Chloride: Chemistry and Technology, Volume 1, "Kalvis" Moscow, Russia, 2008, p. 214-372.
6. S.A. Kurta, N.V. Haber, I.M. Mikitin, Chemical Industry Ukraine 2(55) (2003) 9-14.
7. V.A. Pokrovsky, Absorption Science and Technology 14(5) (1997) 301-307.
8. K. Tanabe, Solid Acids and Bases, Kodansha, Tokyo, 1970, p. 156.
9. G. Leofanti, M. Padovan, M. Garilli, D. Carmello, G.L. Marra, A. Zecchina, G. Spoto, S. Bordiga, Int. J. Mol. Sci. 2 (2001) 244.
10. L. Pauling, General Chemistry, Freeman & Co. San Francisco, 1958, p. 446-448.
11. M. Garilli, P.L. Fatutto, F. Piga, La Chimica e l'Industria 80 (1998) 333.
12. G. Leofanti, A. Marsella, B. Cremaschi, M. Garilli, A. Zecchina, G. Spoto, S. Bordiga, P. Fisicaro, G. Berlier, C. Prestipino, G. Casali, C. Lamberti, J. Catal. 202 (2001) 279.
13. M. Mortensen R.G. Minet, T.T. Tsotsis, Chem. Ing. Sci. 54 (1999) 2131.
14. S.A. Kurta, I.M. Mykytyn, Ukraine Patent 24933. Experimental Setup for Laboratory Simulation of Industrial Process Oxidative Chlorination of Ethylene to 1,2-Dichlorethane, (2006) V01J 10/00, C07C 17/08 (2007.01), declared on 01.02.2007, published Bulletin No. 11, 25.07.2007
15. S.A. Kurta, I.M. Mykytyn, N.V. Haber, J. Appl. Chem. Russia 76(7) (2005) 1110-1113.
16. S.A. Kurta, I.M. Mykytyn, O.S. Kurta, Physics and Chemistry of Solids 9(1) (2008) 143-148.
17. S.A. Kurta, I.M. Mykytyn, O.S Kurta, Physics and Chemistry of Solids 9(3) (2008) 577-582.
18. J. Vall, A. Vargas, M. Firreira , Stud. Surf. Sci. Catal. 7(B) (1981) 1040.
19. P. Avila, J. Blanco, L. Garcia-Fierro, Stud. Surf. Sci. Catal . 7(B) (1981) 1031.
20. C. Zipelli, J.C. Bart, G. Pertini, Z. Anorg. Allg. Chem. 502 (1983) 199.
21. X. Youchang, Z. Huixin, W. Ronghua, Sci. Sin. 23 (1980) 979.
22. U. Nieken, O. Watzenbergen, Chem. Ing. Sci. 54 (1999) 2619.

Tables Captions

Table 1. Differential thermal analysis of γ-Al_2O_3, X1 and MEDC-B catalysts.

Table 2. Diffraction lines angular positions and corresponding inter-planar spacing, d, and relative intensity, I/I_0, for the X1 catalyst.

Table 3. Diffraction lines angular positions and corresponding inter-planar spacing, d, and relative intensity, I/I_0, for the MEDC-B catalyst.

Figures Captions

Figure 1. Infrared spectra from γ-Al_2O_3 carrier, $CuCl_2 \cdot 2H_2O$ and $CuCl_2 \cdot 2HCl$ main catalyst components, industrial MEDC-B and X1 catalysts.

Figure 2. a) Al_2O_3 and copper tetrachloride structures; b) $CuCl_2$ and copper tetrachloride attachment to the Al_2O_3 surface, and $CuCl_2$ linear structure.

Figure 3. Diffraction patterns of $CuCl_2 \cdot 2HCl$ or $H_2[CuCl_4]$ main catalyst components before and after a few days of air exposure.

Figure 4. Diffraction patterns of γ-Al_2O_3, X1 and MEDC-B catalysts as-received and after a few days of air exposure.

Figure 5. Thermal desorption curves of the γ-Al_2O_3 carrier decomposition.

Figure 6. Thermal desorption curves of the MEDC-B catalyst decomposition.

Figure 7. Thermal desorption curves of the X1 catalyst decomposition.

Figure 8. Thermal desorption curves of the $CuCl_2 \cdot H_2O$ active phase decomposition.

Figure 9. Thermal desorption curves of the $CuCl_2 \cdot 2HCl$ or $H_2[CuCl_4]$ active phase decomposition.

Tables

Table 1. Differential thermal analysis of γ-Al_2O_3, X1 and MEDC-B catalysts.

Sample	Beginning/end process temperature			Maximum rate temperature			Process rate, mg/min.			Process weight loss, wt.%			Total weight loss, wt.%	Average weight loss, mg/min
	Drying	Dehydration and dehydro-chlorination	Destruction	Drying	Dehydration and dehydro-chlorination	Destruction	Drying	Dehydration and dehydro-chlorination	Destruction	Drying	Dehydration and dehydro-chlorination	Destruction	All Processes	All Processes
A_2O_3														
No. 2	25/120	120/200	200/590	120	200	480	2.27	1.65	0.34	4.31	2.64	2.64	12.8	0.65
No. 3	50/120	120/250	250/610	120	250	470	2.41	1.81	0.3	3.59	5.02	2.33	11.7	0.28
A_2O_3 Average	37/120	120/225	225/600	120	225	475	2.34	1.73	0.32	3.95	3.83	2.49	12.25	0.47
X1	20/180	180/250	250/550	150	250	525	2.23	2.31	1.97	5.72	2.6	9.49	20.55	1.31
MEDC-B	21/200	200/250	250/690	200	250	640	1.3	3.02	1.28	3.93	2.54	9.48	17.34	1.05

Table 2. Diffraction lines angular positions and corresponding inter-planar spacing, d, and relative intensity, I/I_0, for the X1 catalyst.

No.	2θ, deg.	Intensity I, a.u.	d, Å	I/I_0, %	$\Delta d=d_{X1}-d_{Al2O3}$
1	18.95	1109	4.68293	87.5226	-
2	**19.7**	**1114**	**4.5063**	**88.42676**	**+0.0778**
3	21.75	1108	4.08599	87.34177	-
4	**28.55**	**1071**	**3.12638**	**80.65099**	**+3.1263**
5	29.6	1080	3.01783	82.27848	-
6	30.4	1069	2.94021	80.28933	-
7	31.45	1087	2.8444	83.5443	-
8	**32.4**	**1105**	**2.76314**	**86.79928**	**-0.0167**
9	33.7	1124	2.65946	90.23508	-
10	35.3	1080	2.5425	82.27848	-
11	**36.65**	**1175**	**2.45189**	**99.4575**	**+0.00318**
12	37.5	1141	2.39825	93.30922	-
13	**39.25**	**1074**	**2.29526**	**81.19349**	**+0.0056**
14	40.6	934	2.222	55.87703	-
15	43.15	895	2.09641	48.82459	-
16	**45.9**	**1209**	**1.97701**	**105.60579**	**+0.0060**
17	48.4	852	1.88057	41.04882	-
18	50.1	795	1.82068	30.74141	-
19	52.25	763	1.75071	24.95479	-
20	59.25	824	1.55949	35.98553	-
21	60.45	817	1.53138	34.71971	-
22	61.7	812	1.50332	33.81555	-
23	**66.9**	**1178**	**1.39854**	**100**	**-0.0027**

Table 3. Diffraction lines angular positions and corresponding inter-planar spacing, d, and relative intensity, I/I_0, for the MEDC-B catalyst.

No.	2θ, deg.	Intensity I, a.u.	d, Å	I/I_0, %	$\Delta d=d_{MEDC-B}-d_{Al2O3}$
1	16.95	1092	5.23071	73.39901	-
2	**20.55**	**1150**	**4.32179**	**82.92282**	**-0.1066**
3	23.95	1111	3.71541	76.51888	-
4	**32.6**	**1098**	**2.74664**	**74.38424**	**-0.0332**
5	**37.1**	**1193**	**2.42318**	**89.98358**	**+0.0031**
6	**39.45**	**1094**	**2.28408**	**73.72742**	**-0.0055**
7	45.75	1219	1.98314	94.25287	+0.00122
8	60.5	860	1.53023	35.30378	-
9	**67**	**1254**	**1.3967**	**100**	**-0.0046**

Figures

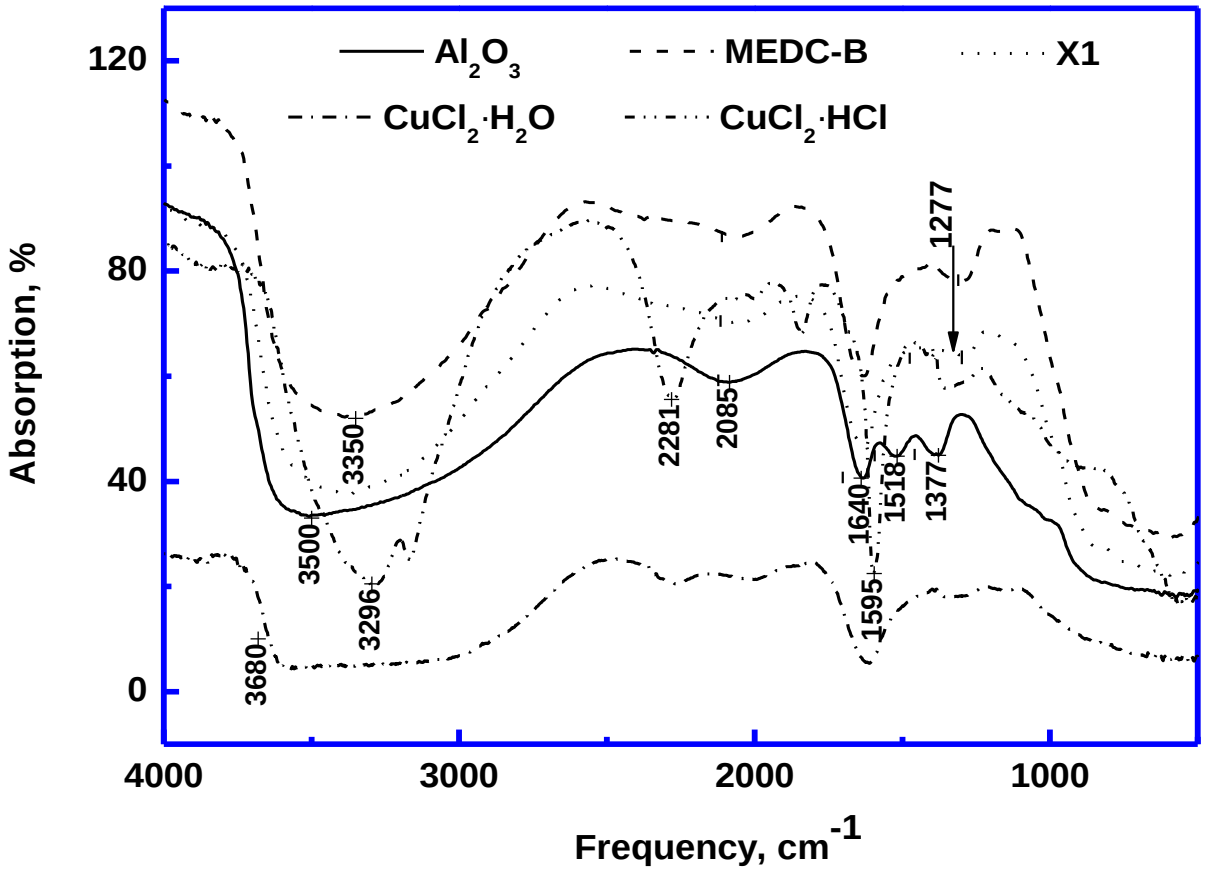

Figure 1. Infrared spectra from γ-Al_2O_3 carrier, $CuCl_2 \cdot 2H_2O$ and $CuCl_2 \cdot 2HCl$ main catalyst components, industrial MEDC-B and X1 catalysts.

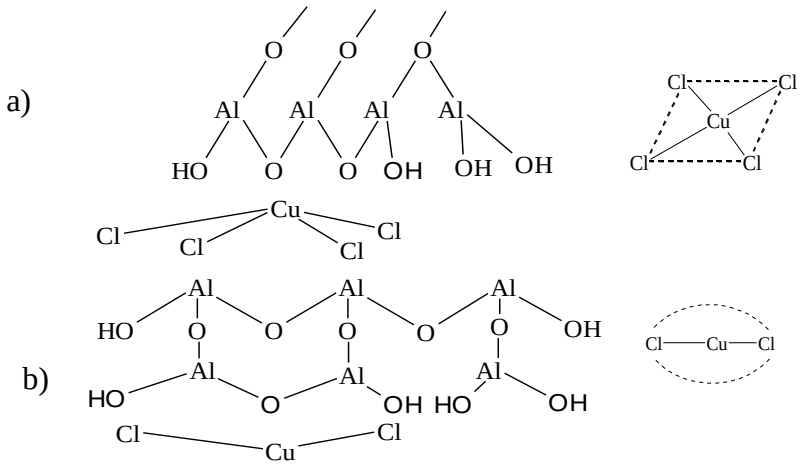

Figure 2. a) Al_2O_3 and copper tetrachloride structures; b) $CuCl_2$ and copper tetrachloride attachment to the Al_2O_3 surface, and $CuCl_2$ linear structure.

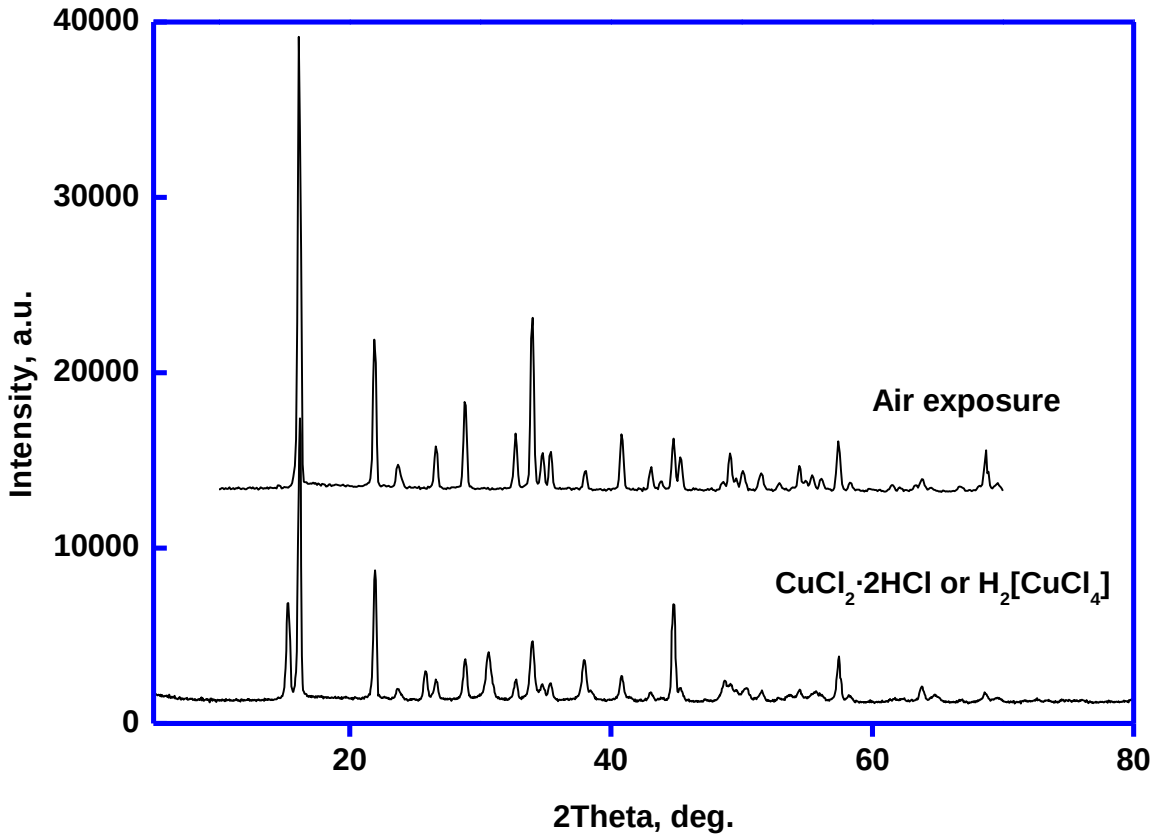

Figure 3. Diffraction patterns of $CuCl_2 \cdot 2HCl$ or $H_2[CuCl_4]$ main catalyst components before and after a few days of air exposure.

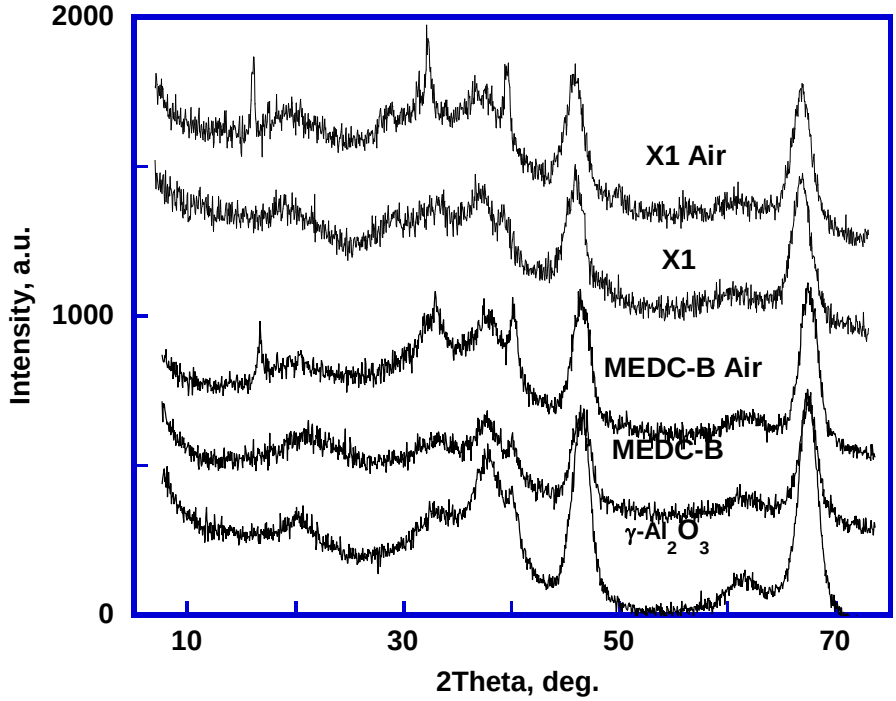

Figure 4. Diffraction patterns of γ-Al_2O_3, X1 and MEDC-B catalysts as-received and after a few days of air exposure.

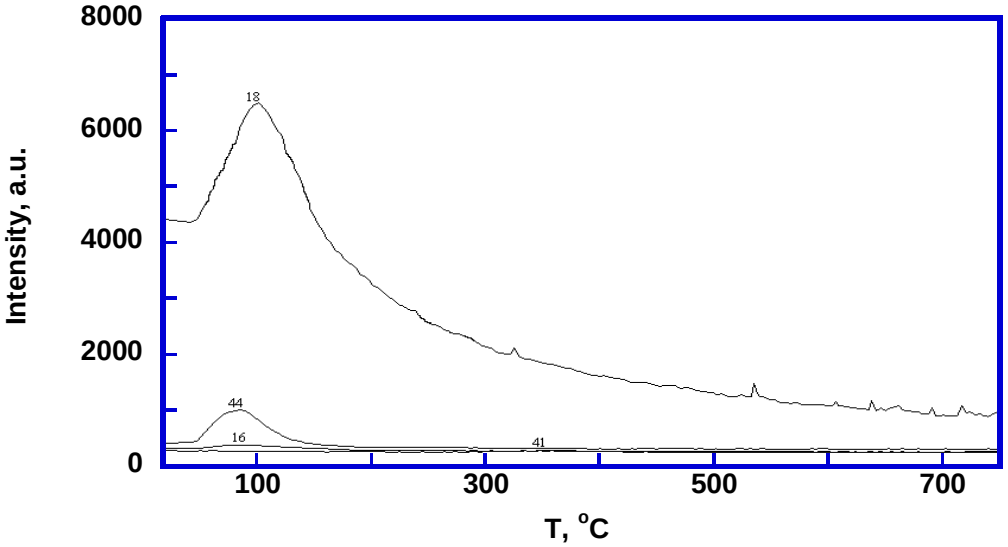

Figure 5. Thermal desorption curves of the γ-Al_2O_3 carrier decomposition.

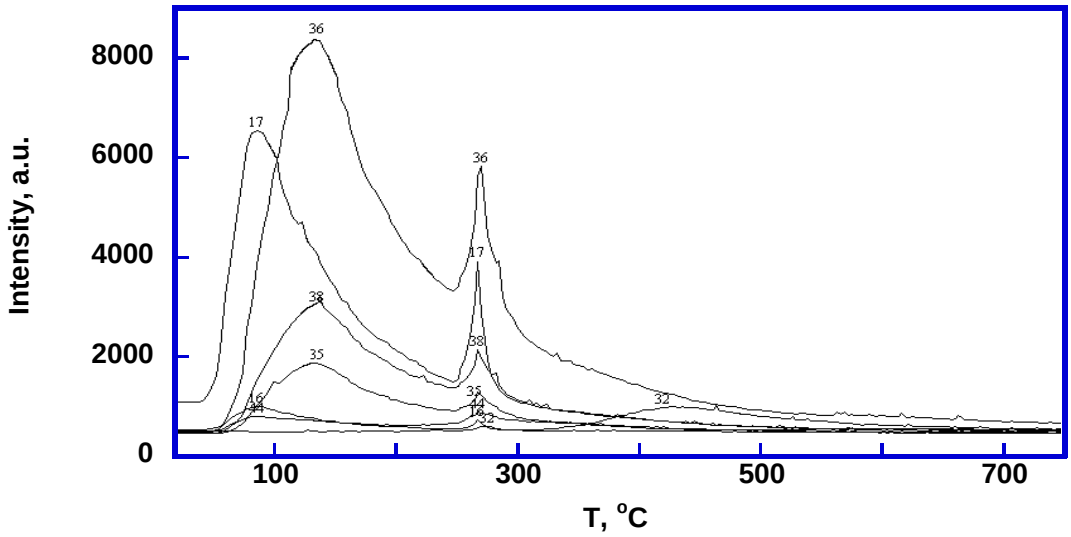

Figure 6. Thermal desorption curves of the MEDC-B catalyst decomposition.

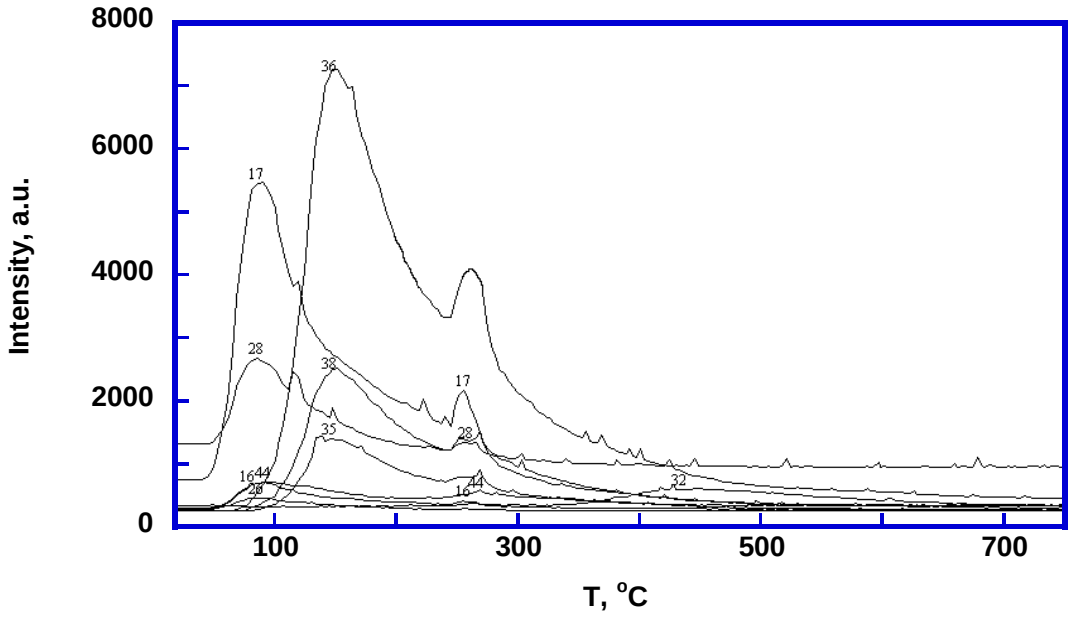

Figure 7. Thermal desorption curves of the X1 catalyst decomposition.

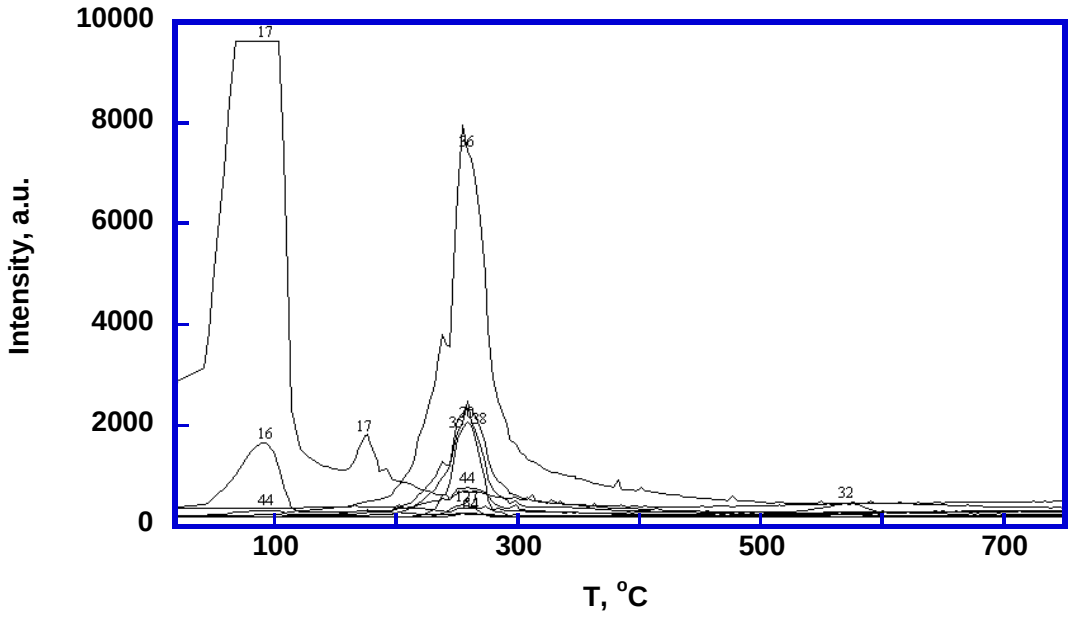

Figure 8. Thermal desorption curves of the $CuCl_2 \cdot H_2O$ active phase decomposition.

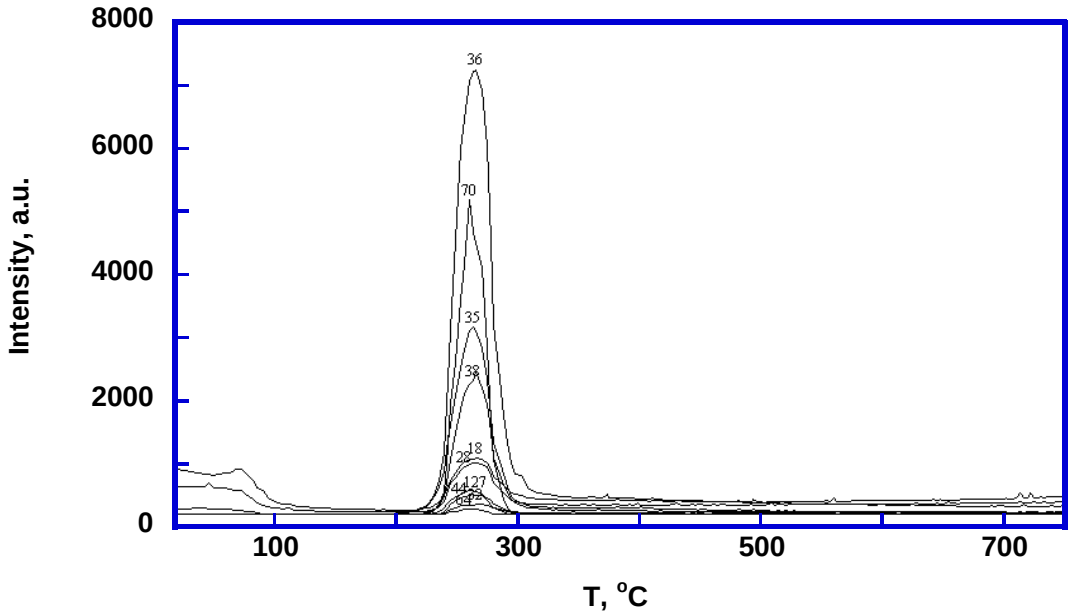

Figure 9. Thermal desorption curves of the $CuCl_2 \cdot 2HCl$ or $H_2[CuCl_4]$ active phase decomposition.